ARTICLE

Continuous Electrical Tuning of the Chemical Composition of TaO_x-Based Memristors

Feng Miao, Wei Yi, Ilan Goldfarb,[†] J. Joshua Yang, Min-Xian Zhang, Matthew D. Pickett, John Paul Strachan, Gilberto Medeiros-Ribeiro,[*] and R. Stanley Williams[*]

Hewlett-Packard Laboratories, 1501 Page Mill Road, Palo Alto, California 94304, United States. [†]On sabbatical leave from Faculty of Engineering, Tel Aviv University, Tel Aviv 69978, Israel.

ABSTRACT TaO_x-based memristors have recently demonstrated both subnanosecond resistance switching speeds and very high write/erase switching endurance. Here we show that the physical state variable that enables these properties is the oxygen concentration in a conduction channel, based on the measurement of the thermal coefficient of resistance of different TaO_x memristor states and a set of reference Ta—O films of known composition. The continuous electrical tunability of the oxygen concentration in the channel, with a resolution of a few percent, was demonstrated by controlling the write currents with a one transistor-one memristor (1T1M) circuit. This study demonstrates that solid-state chemical kinetics is important for the determination of the electrical characteristics of this relatively new class of device.

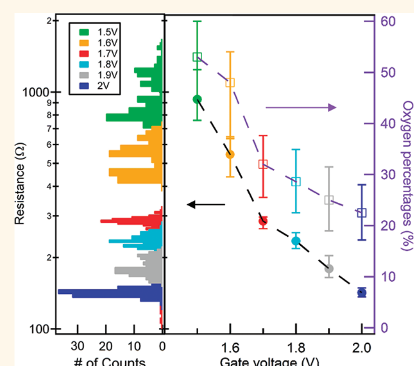

KEYWORDS: memristor · state variable · conduction channel · chemical composition · multilevel storage

Semiconductor doping is a key technology for the precise tuning of resistance in solid state electronic devices, and for the creation of p—n junctions.[1] The doping is metallurgical, and as such determined during the fabrication process.[1,2] Normally, the motion of impurities in an operating semiconductor device is undesirable, unless purposely designed, as in Li:Si devices.[3] However, the coupled motion of charged dopants and carriers in an externally applied electric field within a semiconductor[4−8] has been demonstrated to be a viable mechanism for a memristor.[9−11]

According to the definition formulated by Chua and Kang,[12] the resistance of a generalized memristor (originally called by them a "memristive system", but in the interests of simplifying nomenclature, now just a memristor) is a function of an internal state variable or variables x and may also be a function of either voltage or current according to the quasi-static conduction equation: $V(t) = R(x, I)I(t)$. The state variable is a physical quantity that can be derived from the microscopic properties of the system, and it is explicitly dynamical in nature, that is, the present state is dictated by biasing history, which is described by the dynamical state equation: $dx/dt = f(x, I)$. For example, a TiO_2-based bipolar memristor[13,14] is based on vacancy drift in an externally applied electric field that modulates the tunneling barrier width[15,16] between an electrode and a conduction channel.[17,18] For this system, the dominant state variable is the tunnel gap width.[15] TaO_x based memristors[19−24] have recently demonstrated high endurance (over 10 billion) in terms of write/erase switching cycles,[21,24] and other advantageous features, such as being practically forming-free[14,21] and showing high switching speed (sub-nanosecond).[25] For this particular materials system, the state variable appears to involve the composition (rather than a tunneling gap modulation) of a conduction channel.[26] A better understanding of the device chemistry and physics is required in order to utilize TaO_x-based memristors in novel circuits[27] and memory applications.[28−40]

Here we demonstrate the identification and continuous tunability of the oxygen concentration in the conduction channel core as the dominant state variable in TaO_x-based memristors. We utilized the fact that the thermal coefficient of resistance (TCR) of a Ta—O sample is a geometry-independent property that is a monotonic function of the average oxygen concentration, as determined by electrical and chemical characterizations of reference thin films. The oxygen concentration was determined from

* Address correspondence to gilbertor@hp.com, stan.williams@hp.com.

Received for review November 16, 2011 and accepted February 12, 2012.

Published online February 12, 2012
10.1021/nn2044577

© 2012 American Chemical Society

Rutherford backscattering spectroscopy (RBS) and independently from X-ray photoelectron spectroscopy (XPS) measurements of films that were reactively sputtered with a wide range of oxygen pressures (O/Ta ratios). The TCR of different memristor states was measured and compared to those of the reference Ta–O films. These results showed that the modulation of the oxygen concentration in the conduction channel core in a TaO_x-based memristor was responsible for the resistance switching. Finally, tuning of the states in the TaO_x-based memristors was demonstrated using a simple one transistor-one memristor (1T1M) circuit, which enabled the continuous electrical control of the state variable with a resolution of a few percent in the conduction channel core of the device.

RESULTS AND DISCUSSION

The TaO_x-based memristors consisted of a thin (~18 nm) film of sputtered TaO_x (see Materials and Methods for details), sandwiched between a disk-shaped (~100 μm diameter) Ta top electrode and blanket Pt bottom electrode, as shown schematically in the top inset of Figure 1. The gray dashed curve in Figure 1 corresponds to the first ON switching, which required only a slightly larger voltage than the subsequent ON switching (green curves). After the first ON switching, the resistance of a device was reversibly alternated between the less resistive ON and the more resistive OFF states by the application of a positive and negative voltage, respectively, to the top electrode with the bottom electrode grounded. We see that both the ON and OFF *I*–*V* curves of the device are nearly linear, which means that to a first approximation, the resistance of the memristor is only a function of the state variable *R*(*x*), which significantly simplifies our analysis of this system and indicates that the conduction for all of the states is nearly Ohmic, and thus electron tunneling does not play a significant role in the conductance mechanism for the device.

In the following we show how the O concentration of the conducting region of the memristor can be determined based upon measurements of the material resistivity and TCR. Figure 2a shows the measured TCR of a TaO_x-based memristor (red open square, left *y*-axis) at different resistance states in a 70 Ω to 4 kΩ (bottom *x*-axis) range, which was also the same operating range[41] used to demonstrate high endurance. The TCR here is defined by TCR = $[R(300\text{ K}) - R(T)]/[(300\text{ K} - T) \times R(300\text{ K})]$ for $250\text{ K} < T < 300\text{ K}$, and is a *geometry-independent* quantity that can be compared across samples of various types and sizes. As shown in Figure 2a, the measured TCR was in the range from $5 \times 10^{-4}\text{ K}^{-1}$ to $-1.5 \times 10^{-3}\text{ K}^{-1}$, and decreased continuously as the resistance increased. The crossover from positive to negative TCR occurred around 200–300 Ω, indicating the transition from metallic (positive TCR) to semiconducting (negative TCR) conduction regimes.

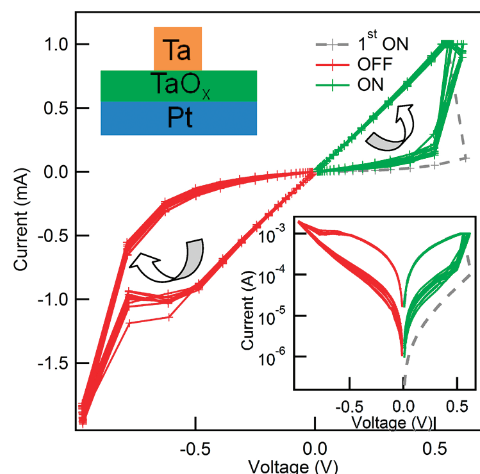

Figure 1. Typical *I*–*V* switching curves of a TaO_x-based memristor including the first ON switching/set (gray dashed curve), the following 10 OFF switching/RESET (red curves) and ON switching/SET (green curves). Inset: same data with the current on a log scale (bottom), and schematic diagram of a typical TaO_x device (top).

The equilibrium binary Ta–O phase diagram contains only two stable phases in the solid state, conducting Ta(O) solid solution and insulating Ta_2O_5.[42] Thus, the TCR and resistivity of an arbitrary Ta–O sample are in principle controlled by a combination of the conducting and the insulating components.[43,44] Gerstenberg *et al.*[43] performed a systematic study of the dependence of TCR on resistivity of thin Ta–O films by adjusting the oxygen concentration of the films (blue hollow diamonds in Figure 2a). We reproduced their results for films prepared in our deposition system (represented by blue solid dots, see Materials and Methods for details). These data correspond to the top *x*-axis of Figure 2a (units of $\mu\Omega\cdot$cm for resistivity). For such a binary system, once the Ta(O) solid solution is supersaturated, Ta_2O_5 begins to precipitate out of solid solution, with the relative amounts of the two determined by the “lever rule”. This precipitation is detected in XPS by the appearance of the Ta^{5+} oxidation state (I. Goldfarb *et al.*, unpublished data), and its onset roughly corresponds to a resistivity of 300–500 $\mu\Omega\cdot$cm (gray band in Figure 2a), from which point onward the dominant conduction mode gradually changes from metallic to semiconducting, and the TCR from positive to negative.

The measured TCR of the TaO_x-based memristor in different states revealed a resistance/resistivity dependence strikingly similar to that of the reference films. Since the resistivity of the reference films was a function of the chemical (oxygen) concentration, we infer that the different resistance states of the device were primarily determined by the chemical (oxygen) concentration of the conduction channel core, and not the changes in the size of the core. As a working model, we assumed that the conduction occurred primarily in an essentially cylindrical core with relatively uniform O

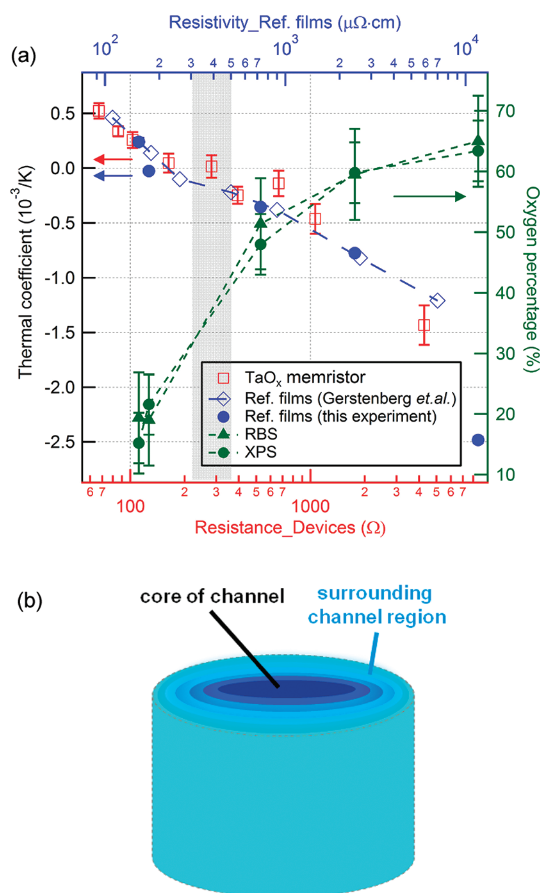

Figure 2. (a) (Left y-axis) TCR (thermal coefficient of resistance) of a TaO_x-based memristor *versus* state resistance (red hollow squares, bottom x-axis); TCR of Ta–O reference films *versus* film resistivity (top x-axis), including comparison of the values measured in this experiment (solid blue dots) and those from the literature (Gerstenberg *et al.*, blue hollow diamonds). The top x-axis is scaled by a calibration factor (1.4) such that the reference sample data follows the same TCR trend as the device data. (Right y-axis) measured oxygen concentration percentage of the reference films by using RBS (dark green solid triangles) and XPS (dark green solid dots) *versus* film resistivity (top x-axis). The alignment of the reference data to the device data is used to estimate the oxygen concentration of the conduction channel core for different device resistances. The gray region corresponds to the threshold values for the appearance of the Ta^{5+} oxidation state in XPS. (b) Schematic illustration of the conduction channel core (dark blue cylinder), which is embedded in the much less conductive surrounding channel region with higher O content (dark blue indicates less O, while light blue indicates more O).

content, which was much more conductive than surrounding material (as illustrated in Figure 2b) because of the stronger than exponential dependence of the resistance on O concentration. To correlate the resistivity measured for the calibration samples with the resistance of the device in a particular state, a geometrical calibration factor reflecting the geometry of the channel ($\alpha = A/L$) was required, such that $\rho = \alpha R$, with R as the resistance, ρ is the resistivity, L is the length and A is the area of the cylindrical core. We can compare the TCR measurements for the calibration films with those for our device in order to determine the calibration factor α by making the following assumptions: (1) the TCR and resistivity are size-independent down to the size of the conduction channel core; (2) the size of any Ta_2O_5 inclusions is small compared to the channel core diameter and/or the number of inclusions is negligible for the range of concentrations investigated in this study. Thus by utilizing the oxide film thickness as an upper bound for L, we can estimate the radius of the core of the conduction channel if we fit the resistance with one fitting parameter $\alpha = (1.4 \pm 0.3) \times 10^{-8}$ m. The TCR curves of both systems are shown in Figure 2a utilizing the fitted α to combine the resistivity and resistance data on a single plot. We obtained good agreement for the metallic states, as well as the transition regime for TCR in the range between 0 and -5×10^{-4} K^{-1}, beyond which the assumption for Ta_2O_5 inclusions may fail. Since the TCR is determined by the chemical composition of a Ta–O film, we conclude that the resistance switching is primarily caused by the modulation of the chemical concentration in the conduction channel. Using the known film thickness as the upper limit for the conduction channel thickness, we can infer a radius of ~9 ± 1 nm for the channel core, which is almost 4 orders of magnitude smaller than the radius of the fabricated device. In actuality, there was most likely a concentration gradient rather than an abrupt change from a constant low to high O composition in the channel region; however, given the strong dependence of the resistance on composition, the general conclusions based on our working model remain valid, as determined by performing a sensitivity analysis (see Supporting Information).

The reference films were utilized to independently calibrate the average chemical concentration of the conduction channel core of TaO_x-based memristors. Both RBS and XPS measurements (see Materials and Methods for details) were performed to measure the oxygen concentration percentage in the calibration films, and the results are plotted on the right y-axis of Figure 2a (green markers) as a function of film resistivity (top x-axis). These two independent techniques agreed within 5% on the oxygen concentration. As expected, increasing oxygen concentration caused a corresponding increase in resistivity. The fitting procedure of α allows scaling of the top abscissa (resistivity) with the bottom one (resistance state), and more importantly, correlates the latter with the O concentration of the conduction channel core. We conclude that switching in the operation range (~100 Ω to 4 kΩ) corresponds to a variation of the oxygen concentration in the core of the channel between ~15% and ~62%. Nominally identical devices analyzed by pressure-modulated conductance microscopy (PMCM),[26,45–47] cross-sectional transmission electron microscopy (TEM)[26] and X-ray spectromicroscopy,[48] confirm the existence of a conductive channel core with relatively low oxygen

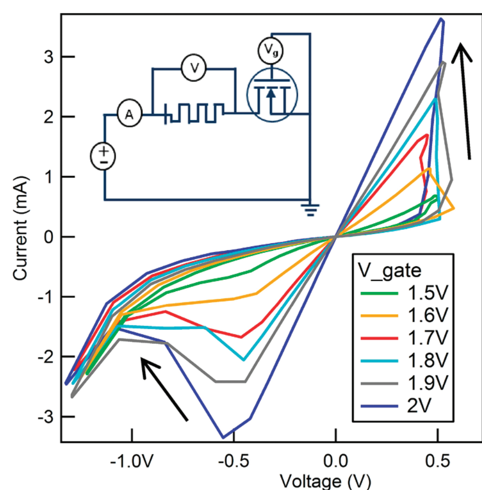

Figure 3. Demonstration of continuous electrical tuning of the resistance states (and thus the chemical concentrations) of the memristor conductance channel with 1T1M circuitry: *I*−*V* switching curves with constant writing voltages (1 V and −1.5 V) at different gate voltages (arrows indicating switching polarities). Inset: 1T1M circuit diagram.

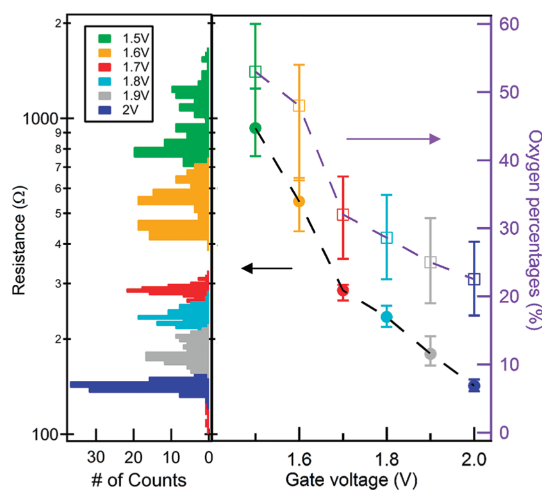

Figure 4. Left: Histogram of ON state resistance for different gate voltages (represented by different colors). Right: median value (solid dots) with the 10th and 90th percentiles (error bars) of ON state resistances for 100 cycles, and the estimated oxygen concentration percentage (hollow squares, right *y*-axis) of the conduction channel as a function of gate voltage applied during the ON switching processes. The value and error bars of the oxygen concentration percentage were estimated from the median value and the 10th and 90th percentiles of ON state resistance using the reference curves in Figure 2a.

concentration, surrounded by a much less conductive channel region with a high oxygen concentration (the entire channel region had a radius *ca.* 50−100 nm). While a precise measurement of the actual size of the nanoscale conduction channel core in a functioning device is extremely challenging, the TCR study provided an indirect yet plausible estimate.

The above analysis allows us to conclude that there is a large range of chemical concentration and resistance that can be deterministically accessed within our devices, for which the state variable of the device is the O concentration. An open-loop electronic method to tune the O concentration in the channel can be implemented using a 1T1M circuit. By driving the transistor from the linear into the saturation regime, we can limit the current through the memristor, that is, implement current-compliance. The 1T1M write circuitry[49,50] is shown in the inset of Figure 3. A standard 4-probe setup was used to switch the memristor with a NMOS field effect transistor (FET) connected in series. When the memristor was positively biased, the maximum current flow in the circuit was limited by the saturation current of the NMOS FET, controlled *via* gate voltage. When the device was negatively biased, the NMOS FET served simply as a series resistor (∼45 Ω). The ON and OFF switching curves with constant writing voltages (1 and −1.5 V, respectively) at different gate voltages (1.5−2 V with an interval of 0.1 V) are shown in Figure 3. When a 1 V writing voltage was applied to switch the device to ON states, different gate voltages yielded different current compliances and thus different final resistances (which changed monotonically with the gate voltages). After each ON-switching operation, the device was switched back to the same initial OFF state (with resistance at ∼2.5 KΩ) by applying a −1.5 V RESET voltage. To evaluate the stochastic nature of the ON-switching operation, a statistical study of the ON resistance states was performed. Results for 100 sequential switching events for each gate voltage are shown in the histogram of Figure 4. The median state resistances are plotted (solid dots, left *y*-axis), with error bars representing the 10th and 90th percentiles of the measured distribution, as a function of gate voltage in the right panel of Figure 4. The higher resistance states had a larger variance, while lower resistance states (∼140 to 300 Ω) had very narrow distributions and excellent controllability. In this test, the NMOS FET gate voltages were monotonically increased, and in a subsequent test (not shown), they were randomly chosen, with both experiments producing essentially the same results.

Furthermore, we can estimate the oxygen concentration percentage in the core of the conduction channel for each gate-voltage-controlled switching current. In the following, we used the median state resistance for each gate voltage, as shown in Figure 4. The average oxygen concentration percentage for the cylinder-shaped channel core was estimated from the reference curves in Figure 2a, and the results are shown in the right graph of Figure 4 (hollow squares, right *y*-axis). When the gate voltage was changed from 1.5 to 2 V, the oxygen concentration of the channel core was tuned from about 53% to 21%. A significant change of about 16% was observed when gate voltage was changed from 1.7 to 1.6 V. This abrupt change most likely corresponded to the oxygen solubility limit of

Ta(O) and the appearance of the Ta^{5+} oxidation state in the core of the conduction channel, which in thin amorphous films was reported to substantially exceed that in the bulk, by up to ~20%.[43] Below this gate voltage (1.6 V), we also observed wider distributions in the histogram of resistance, as shown in Figure 4. Using the 9 nm radius, 18 nm height of the channel core and the concentration of oxygen in the core, we can roughly estimate the average number of oxygen atoms that is controlled by the gate voltage. For example, when the gate voltage decreased from 2 to 1.7 V, the oxygen content in the channel core increased from $\sim 6.7 \times 10^4$ to $\sim 1.2 \times 10^5$ atoms. The relatively small number of O atoms and their varying spatial distributions are responsible for the stochastic variations observed in the ON-switching operations performed for different gate voltages.

The identification and measurement of the oxygen concentration as the state variable in TaO_x-based memristors offers a platform for future kinetics studies of the chemically mobile species. Simultaneous measurements of the current and voltage as functions of time of a memristor,[12,51] along with the resistance dependence on the oxygen concentration, will enable an experimental determination of the rate of change of the oxygen concentration, dx/dt, for times into the subnanosecond scale.[16,25] By examining the current and/or voltage dependence of this rate, one can determine the functional form for the memristor dynamical equation.[15] Thus, understanding the kinetics of the chemically mobile species during the switching process, which is influenced by factors such as field drift, Fick diffusion, and thermophoresis (D. Strukov *et al.*, unpublished data), is a crucial step in accurate device and circuit modeling involving memristors.

CONCLUSIONS

In summary, we have demonstrated a mixed conduction device – ionic and electronic – in which we can deterministically utilize the former process to control the latter. For these TaO_x-based memristors, we identified the oxygen concentration of the core region of the conduction channel as the dominant state variable. We calibrated the oxygen concentration within the core of the conduction channel by correlating the TCR data taken from different states of a TaO_x-based memristor to RBS and XPS data from reference Ta–O films with known compositions. Finally, by utilizing 1T1M write circuitry, we successfully implemented continuous tunability of the state variable, the oxygen concentration in the channel, through applying different gate voltages. These results indicate that feedback schemes proposed recently[52–54] can be utilized to control the state variable. These finding show not only that the scalability of this system is promising (~18 nm diameter), but multilevel states can be realized in a device. Combined with the low switching power and high endurance characteristics, these attributes make TaO_x-based memristors attractive for nonvolatile memory and storage applications.

MATERIALS AND METHODS

TaO_x Devices and Reference Films. The TaO_x film utilized in the devices was sputtered from a tantalum oxide target (nominal composition $TaO_{2.0}$) with an Ar gas pressure of about 3 mTorr. The substrate for the devices was 200 nm SiO_2 on a Si wafer. The device stack consisted of (from bottom to up) 1 nm Ti blanket adhesion layer, 100–400 nm Pt blanket bottom electrode, 18 nm TaO_x blanket layer, and 100–400 nm thick Ta disk (100 μm diameter) top electrodes. The reference Ta–O films (100–200 nm on a substrate of 110 nm SiO_2 on Si wafer) were RF-sputtered from a Ta target in an AJA International, Inc. magnetron sputtering system, with 150 W at a dynamic pressure 8 mTorr, Ar flow rate 20 sccm (standard cubic centimeters per minute), and O_2 flow rate varying from 0 to 1 sccm. The vacuum of the chamber before gas introduction was $\sim 2 \times 10^{-8}$ mbar. The substrate temperature during the deposition was held at ~700 K.

Electrical Measurements. The $I-V$ switching curves and resistance measurements were performed with an Agilent B1500A parameter analyzer. With the setup of short integration time and autogain, the measurement interval time varies between few and tens of milliseconds. The temperature in a Janis cryostat was ramped up and down between 250 and 300 K in nine steps with equal interval for determination of the TCR. Square shaped (5 mm × 5 mm) samples of Ta–O reference films with contact pads (10 nm Ti covered by 30 nm Pt) at the corners were used for the resistivity measurements in a van der Pauw configuration.

RBS and XPS Measurements. Sample thickness and average oxygen concentration were obtained from RBS (by Evans Analytical Group), which showed a uniform composition profile over the entire film thickness. The oxygen concentration of the near surface region of the films was also measured by weighting the sum of the all the components from deconvolution of the Ta 4f core-level XPS spectra. The XPS measurements were performed immediately after the deposition in an *in situ* analysis chamber (6×10^{-10} mbar base pressure). XPS analysis employed a monochromated Al anode (1486.7 eV) and EIS-SPHERA hemispherical analyzer by Omicron Nanotechnology, GmbH.

Conflict of Interest: The authors declare no competing financial interest.

Acknowledgment. We thank J. Borghetti for stimulating discussions. This research was supported in part by the SyNAPSE program of the Defense Advanced Research Projects Agency under contract HR0011-09-3-0001. The views, opinions, and/or findings contained in this article are those of the authors and should not be interpreted as representing the official views or policies, either expressed or implied, of the Defense Advanced Research Projects Agency or the Department of Defense.

Supporting Information Available: This section includes sensitivity analysis of the estimation of the calibration factor, a second set of TCR data from another TaO_x-based memristor and estimation of the radius of the channel core assuming exponential dependence of conductivity on composition. This material is available free of charge *via* the Internet at http://pubs.acs.org.

REFERENCES AND NOTES

1. Hall, R. N.; Dunlap, W. C. P–N Junctions Prepared by Impurity Diffusion. *Phys. Rev.* **2008**, *80*, 467–468.

2. Shockley, W. *Electrons and Holes in Semiconductors: With Applications to Transistor Electronics*; D. Van Nostrand: New York, 1959.
3. Fuller, C. S.; Severiens, J. C. Mobility of Impurity Ions in Germanium and Silicon. *Phys. Rev.* **1954**, *96*, 21–24.
4. Nafe, H. Current−Voltage Relation and Charge Distribution in Mixed Ionic−Electronic Solid Conductors. *J. Electrochem. Soc.* **1997**, *144*, 3922–3929.
5. Singh, R.; Jacob, K. T. Solution of Transport Equations in a Mixed Conductor—A Generic Approach. *Int. J. Eng. Sci.* **2004**, *42*, 1587–1602.
6. Meyer, R.; Liedtke, R.; Waser, R. Oxygen Vacancy Migration and Time-Dependent Leakage Current Behavior of $Ba_{0.3}Sr_{0.7}TiO_3$ Thin Films. *Appl. Phys. Lett.* **2005**, *86*, 112904–112906.
7. Kwon, H. I.; Ravaioli, U. Simulation of Electronic/Ionic Mixed Conduction in Solid Ionic Memory Devices. *Microelectron. J.* **2006**, *37*, 1047–1051.
8. Gil, Y.; Umurhan, O. M.; Tsur, Y.; Riess, I. Recent Calculations and Measurements of *I*−*V* Relations in Simple Devices Based on Thin Nano *versus* Thick Layers of Semiconductors with Mobile Acceptors or Donors. *Solid State Ionics* **2008**, *179*, 1187–1193.
9. Chua, L. Memristor-The Missing Circuit Element. *IEEE Trans. Circuit Theory* **1971**, *CT-18*, 507–519.
10. Strukov, D.; Snider, G.; Stewart, D.; Williams, R. S. The Missing Memristor Found. *Nature* **2008**, *453*, 80–83.
11. Strukov, D.; Borghetti, J.; Williams, R. S. Coupled Ionic and Electronic Transport Model of Thin-Film Semiconductor Memristive Behavior. *Small* **2009**, *5*, 1058–1063.
12. Chua, L.; Kang, S. Memristive Devices and System. *Proc. IEEE* **1976**, *64*, 209–223.
13. Yang, J. J.; Pickett, M. D.; Li, X.; Ohlberg, D.; Stewart, D.; Williams, R. S. Memristive Switching Mechanism for Metal/Oxide/Metal Nanodevices. *Nat. Nanotechnol.* **2008**, *3*, 429–433.
14. Yang, J. J.; Miao, F.; Pickett, M. D.; Ohlberg, D. A. A.; Stewart, D. R.; Lau, C. N.; Williams, R. S. The Mechanism of Electroforming of Metal Oxide Memristive Switches. *Nanotechnology* **2009**, *20*, 215201.
15. Pickett, M. D.; Strukov, D.; Borghetti, J.; Yang, J. J.; Snider, G.; Stewart, D.; Williams, R. S. Switching Dynamics in Titanium Dioxide Memristive Devices. *J. Appl. Phys.* **2009**, *106*, 074508.
16. Miao, F.; Yang, J. J.; Strachan, J. P.; Stewart, D.; Williams, R. S.; Lau, C. N. Force Modulation of Tunnel Gaps in Metal Oxide Memristive Nanoswitches. *Appl. Phys. Lett.* **2009**, *95*, 113503.
17. Kwon, D.-H.; Kim, K.; Jang, J.; Jeon, J.; Lee, M.; Kim, G.; Li, X.-S.; Park, G.-S.; Lee, B.; Han, S.; *et al.* Atomic Structure of Conducting Nanofilaments in TiO_2 Resistive Switching Memory. *Nat. Nanotechnol.* **2010**, *5*, 148–153.
18. Strachan, J. P.; Pickett, M. D.; Yang, J. J.; Aloni, S.; Kilcoyne, D.; Medeiros-Ribeiro, G.; Williams, R. S. Direct Identification of the Conducting Channels in a Functioning Memristive Device. *Adv. Mater. (Weinheim, Germany)* **2010**, *22*, 3573–3577.
19. Wei, Z.; Kanzawa, Y.; Arita, K.; Katoh, Y.; Kawai, K.; Muraoka, S.; Mitani, S.; Fujii, S.; Katayama, K.; Iijima, M.; *et al*. Highly Reliable TaO_x ReRAM and Direct Evidence of Redox Reaction Mechanism. *IEDM Tech. Dig.* **2008**, *1*, 1–4.
20. Terai, M.; Sakotsubo, Y.; Kotsuji, S.; Hada, H. Resistance Controllability of Ta_2O_5/TiO_2 Stack ReRAM for Low-Voltage and Multilevel Operation. *IEEE Electron Device Lett.* **2010**, *31*, 204–206.
21. Yang, J. J.; Zhang, M. X.; Strachan, J. P.; Miao, F.; Pickett, M. D.; Kelley, R. D.; Medeiros-Ribeiro, G.; Williams, R. S. High Switching Endurance in TaO_x Memristive Devices. *Appl. Phys. Lett.* **2010**, *97*, 232102.
22. Tsuji, Y.; Sakamoto, T.; Banno, N.; Hada, H.; Aono, M. Off-State and Turn-On Characteristics of Solid Electrolyte Switch. *Appl. Phys. Lett.* **2010**, *96*, 023504.
23. Lee, C. B.; Lee, D. S.; Benayad, A.; Lee, S. R.; Chang, M.; Lee, M.-J.; Hur, J.; Kim, Y. B.; Kim, C. J.; Chung, U.-I. Highly Uniform Switching of Tantalum Embedded Amorphous Oxide Using Self-Compliance Bipolar Resistive Switching. *IEEE Electron Device Lett.* **2011**, *32*, 399–401.
24. Lee, M.-J.; Lee, C. B.; Lee, D.; Lee, S. R.; Chang, M.; Hur, J. H.; Kim, Y.-B.; Kim, C.-J.; Seo, D. H.; Seo, S.; *et al.* A Fast, High-Endurance and Scalable Non-volatile Memory Device Made from Asymmetric Ta_2O_{5-x}/TaO_{2-x} Bilayer Structures. *Nat. Mater.* **2011**, *10*, 625–630.
25. Torrezan, A. C.; Strachan, J. P.; Medeiros-Ribeiro, G.; Williams, R. S. Sub-nanosecond Switching of Tantalum Oxide Memristor. *Nanotechnology* **2011**, *22*, 485203.
26. Miao, F.; Strachan, J. P.; Yang, J. J.; Zhang, M.-X.; Goldfarb, I.; Torrezan, A. C.; Eschbach, P.; Kelley, R. D.; Medeiros-Ribeiro, G.; Williams, R. S. Anatomy of a Nanoscale Conduction Channel Reveals the Mechanism of a High-Performance Memristor. *Adv. Mater. (Weinheim, Germany)* **2011**, *23*, 5633–5640.
27. Snider, G. S. Spike-Timing-Dependent Learning in Memristive Nanodevices. *IEEE Int. Symp. Nanoscale Arch.* **2008**, 85.
28. Waser, R.; Aono, M. Nanoionics-Based Resistive Switching Memories. *Nat. Mater.* **2007**, *6*, 833–840.
29. Waser, R.; Dittmann, R.; Staikov, G.; Szot, K. Redox-Based Resistive Switching Memories- Nanoionic Mechanisms, Prospects, and Challenges. *Adv. Mater. (Weinheim, Germany)* **2009**, *21*, 2632–2663.
30. Sawa, A. Resistive Switching in Transition Metal Oxides. *Mater. Today* **2008**, *11*, 28–36.
31. Kozicki, M. N.; Park, M.; Mitkova, M. Nanoscale Memory Elements based on Solid-State Electrolytes. *IEEE Trans. on Nanotechnol.* **2005**, *4*, 331–338.
32. Meijer, G. I. Who Wins the Nonvolatile Memory Race? *Science* **2008**, *319*, 1625–1626.
33. Nishi, Y.; Jameson, J. Challenge of Nanoelectronic Materials and Devices toward New Nonvolatile Memories. *9th Int. Conf. Solid-State Integrated-Circuit Technol.* **2008**, *1*−*4*, 891–896.
34. McCreery, R. L. Molecular Electronic Junctions. *Chem. Mater.* **2004**, *16*, 4477–4496.
35. Rozenberg, M. J.; Inoue, I. H.; Sanchez, M. J. Nonvolatile Memory with Multilevel Switching: A Basic Model. *Phys. Rev. Lett.* **2004**, *92*, 178302.
36. Schindler, C.; Thermadam, S. C. P.; Waser, R.; Kozicki, M. N. Bipolar and Unipolar Resistive Switching in Cu-Doped SiO_2. *IEEE Trans. Electron Devices* **2007**, *54*, 2762–2768.
37. Terabe, K.; Hasegawa, T.; Nakayama, T.; Aono, M. Quantized Conductance Atomic Switch. *Nature* **2005**, *433*, 47–50.
38. Gergel-Hackett, N.; Hamadani, B.; Dunlap, B.; Suehle, J.; Richter, C.; Hacker, C.; Gundlach, D. A Flexible Solution-Processed Memristor. *IEEE Electron Device Lett.* **2009**, *30*, 706–708.
39. Yang, J. J.; Borghetti, J.; Murphy, D.; Duncan, D. R.; Williams, R. S. A Family of Electronically Reconfigurable Nanodevices. *Adv. Mater. (Weinheim, Germany)* **2009**, *21*, 1–5.
40. The International Technology Roadmap for Semiconductors. Emerging Research Devices, Technical report, **2009**.
41. Some TaO_x devices also show a more resistive operation range of ∼10 KΩ to several 100 KΩ with much less reliable performances on endurance. Thus in this work we focus on the more conductive operation range with ultrahigh endurance only.
42. Garg, S. P.; Krishnamurthy, N.; Awasthi, A.; Venkatraman, M. The O−Ta (Oxygen−Tantalum) System. *J. Phase Equilib.* **1996**, *17*, 63–77.
43. Gerstenberg, D.; Calbick, C. J. Effects of Nitrogen, Methane, and Oxygen on Structure and Electrical Properties of Thin Tantalum Films. *J. Appl. Phys.* **1964**, *35*, 402–407.
44. Ichinohe, T.; Masaki, S.; Uchida, K.; Nozaki, S.; Morisaki, H. Fabrication of Nanostructured Palladium-Doped SiO_2 Films with Variable Temperature Coefficient of Resistivity. *Thin Solid Films* **2004**, *466*, 27–33.
45. Lau, C. N.; Stewart, D. R.; Williams, R. S.; Bockrath, M. Direct Observation of Nanoscale Switching Centers in Metal/Molecule/Metal Structures. *Nano Lett.* **2004**, *4*, 569–572.
46. Miao, F.; Ohlberg, D.; Stewart, D. R.; Williams, R. S.; Lau, C. N. Quantum Conductance Oscillations in Metal/Molecule/Metal Switches at Room Temperature. *Phys. Rev. Lett.* **2008**, *101*, 016802.

47. Miao, F.; Ohlberg, D.; Williams, R. S.; Lau, C. N. Characterization of Quantum Conducting Channels in Metal/Molecule/Metal Devices using Pressure-Modulated Conductance Microscopy. *Appl. Phys. A: Mater. Sci. Process.* **2011**, *102*, 943–948.
48. Strachan, J. P.; Medeiros-Ribeiro, G.; Yang, J. J.; Zhang, M.-X.; Miao, F.; Goldfarb, I.; Holt, M.; Rose, V.; Williams, R. S. Spectromicroscopy of Tantalum Oxide Memristors. *Appl. Phys. Lett.* **2011**, *98*, 242114.
49. Kinoshita, K.; Tsunoda, K.; Sato, Y.; Noshiro, H.; Yamazaki, Y.; Fukano, T.; Yagaki, S.; Aoki, M.; Sugiyama, Y. Reduction of Reset Current in NiO-ReRAM Brought about by Ideal Current Limiter. *Nonvol. Semicond. Mem. Workshop* **2007**, 66–67.
50. Lee, H. Y.; Chen, P. S.; Wu, T. Y.; Chen, Y. S.; Wang, C. C.; Tzeng, P. J.; Lin, C. H.; Chen, F.; Lien, C. H.; Tsai, M.-J. Low Power and High Speed Bipolar Switching with a Thin Reactive Ti Buffer Layer in Robust HfO_2 Based RRAM. *IEDM Tech. Dig.* **2008**, 297–300.
51. Chua, L. Resistance Switching Memories Are Memristors. *Appl. Phys. A: Mater. Sci. Process.* **2011**, *102*, 765–783.
52. Yi, W.; Perner, F.; Qureshi, M. S.; Abdalla, H.; Pickett, M. D.; Yang, J. J.; Zhang, M.-X.; Medeiros-Ribeiro, G.; Williams, R. S. Feedback Write Scheme for Memristive Switching Devices. *Appl. Phys. A: Mater. Sci. Process.* **2011**, *102*, 973–982.
53. Medeiros-Ribeiro, G.; Perner, F.; Carter, R.; Abdalla, H.; Pickett, M. D.; Williams, R. S. Lognormal Switching Times for Titanium Dioxide Bipolar Memristors: Origin and Resolution. *Nanotechnology* **2011**, *22*, 095702.
54. Alibart, F.; Gao, L.; Hoskins, B. D.; Strukov, D. B. High Precision Tuning of State for Memristive Devices by Adaptable Variation-Tolerant Algorithm. *Nanotechnology* **2012**, *23*, 075201.